Chapter 7

The synapse

This chapter covers a spectrum of models for both chemical and electrical synapses. Different levels of detail are delineated in terms of model complexity and suitability for different situations. These range from empirical models of voltage waveforms to more detailed kinetic schemes, and to complex stochastic models, including vesicle recycling and release. Simple static models that produce the same postsynaptic response for every presynaptic action potential are compared with more realistic models incorporating short-term dynamics that produce facilitation and depression of the postsynaptic response. Different postsynaptic receptor mediated excitatory and inhibitory chemical synapses are described. Electrical connections formed by gap junctions are considered.

7.1 Synaptic input

So far we have considered neuronal inputs in the form of electrical stimulation via an electrode, as in an electrophysiological experiment. Many neuronal modelling endeavours start by trying to reproduce the electrical activity seen in particular experiments. However, once a model is established on the basis of such experimental data, it is often desired to explore the model in settings that are not reproducible in an experiment. For example, how does the complex model neuron respond to patterns of synaptic input? How does a model network of neurons function? What sort of activity patterns can a network produce? These questions, and many others besides, require us to be able to model synaptic input. We discuss chemical synapses in most detail as they are the principal mediators of targeted neuronal communication. Electrical synapses are discussed in Section 7.7.

The **chemical synapse** is a complex signal transduction device that produces a postsynaptic response when an action potential arrives at the presynaptic terminal. A schematic of the fundamental components of a chemical synapse is shown in Figure 7.1. We describe models of chemical synapses based on the conceptual view that a synapse consists of one or more active zones that contain a presynaptic readily releasable vesicle pool (RRVP)

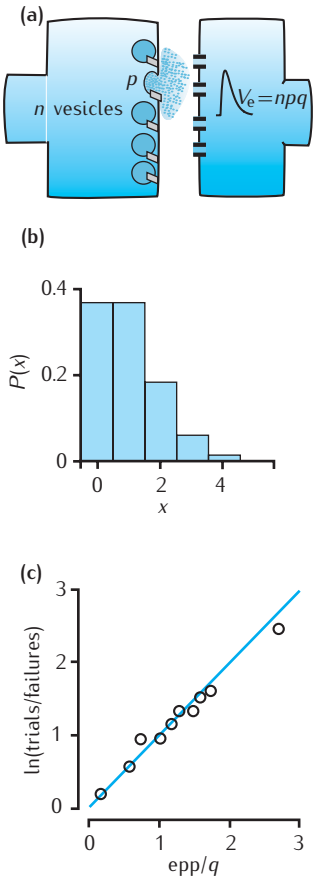

Fig. 1.2 **(a)** Quantal hypothesis of synaptic transmission. **(b)** Example Poisson distribution of the number of released quanta when $m = 1$. **(c)** Relationship between two estimates of the mean number of released quanta at a neuromuscular junction. Blue line shows where the estimates would be identical. Plotted from data in Table 1 of Del Castillo and Katz (1954a), following their Figure 6.

Box 1.2 Reasoning with models

An example in neuroscience where mathematical models have been key to reasoning about a system is chemical synaptic transmission. Though more direct experiments are becoming possible, much of what we know about the mechanisms underpinning synaptic transmission must be inferred from recordings of the postsynaptic response. Statistical models of neurotransmitter release are a vital tool.

In the 1950s, the **quantal hypothesis** was put forward by Del Castillo and Katz (1954a) as an aid to explaining data obtained from frog neuromuscular junctions. Release of acetylcholine at the nerve–muscle synapse results in an **endplate potential** (**EPP**) in the muscle. In the absence of presynaptic activity, spontaneous **miniature endplate potentials** (**MEPPs**) of relatively uniform size were recorded. The working hypothesis was that the EPPs evoked by a presynaptic action potential actually were made up by the sum of very many MEPPs, each of which contributed a discrete amount, or 'quantum', to the overall response. The proposed underlying model is that the mean amplitude of the evoked EPP, V_e, is given by:

$$V_e = npq,$$

where n quanta of acetylcholine are available to be released. Each can be released with a mean probability p, though individual release probabilities may vary across quanta, contributing an amount q, the **quantal amplitude**, to the evoked EPP (Figure 1.2a).

To test their hypothesis, Del Castillo and Katz (1954a) reduced synaptic transmission by lowering calcium and raising magnesium in their experimental preparation, allowing them to evoke and record small EPPs, putatively made up of only a few quanta. If the model is correct, then the mean number of quanta released per EPP, m, should be:

$$m = np.$$

Given that n is large and p is very small, the number released on a trial-by-trial basis should follow a Poisson distribution (Appendix B.3) such that the probability that x quanta are released on a given trial is (Figure 1.2b):

$$P(x) = (m^x/x!)exp(-m).$$

This leads to two different ways of obtaining a value for m from the experimental data. Firstly, m is the mean amplitude of the evoked EPPs divided by the quantal amplitude, $m \equiv \overline{V}_e/q$, where q is the mean amplitude of recorded miniature EPPs. Secondly, the recording conditions result in many complete failures of release, due to the low release probability. In the Poisson model the probability of no release, $P(0)$, is $P(0) = \exp(-m)$, leading to $m = -\ln(P(0))$. $P(0)$ can be estimated as (number of failures)/(number of trials). If the model is correct, then these two ways of determining m should agree with each other:

$$m \equiv \overline{V}_e/q = \ln \frac{\text{trials}}{\text{failures}}.$$

Plots of the experimental data confirmed that this was the case (Figure 1.2c), lending strong support for the quantal hypothesis.

Such **quantal analysis** is still a major tool in analysing synaptic responses, particularly for identifying the pre- and postsynaptic loci of biophysical changes underpinning short- and long-term synaptic plasticity (Ran *et al.*, 2009; Redman, 1990). More complex and dynamic models are explored in Chapter 7.

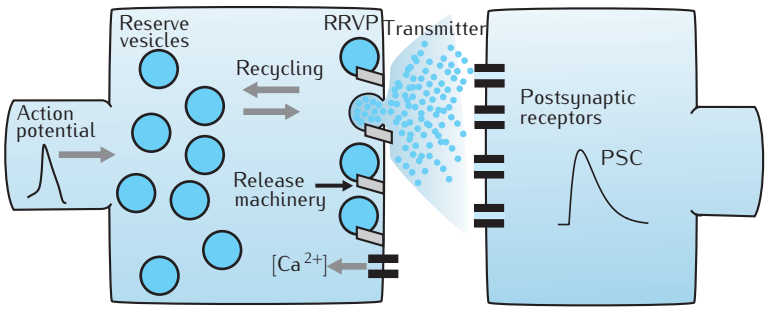

Fig. 7.1 Schematic of a chemical synapse. In this example, the presynaptic terminal consists of a single active zone containing a RRVP which is replenished from a single reserve pool. A presynaptic action potential leads to calcium entry through voltage-gated calcium channels which may result in a vesicle in the RRVP fusing with the presynaptic membrane and releasing neurotransmitter into the synaptic cleft. Neurotransmitter diffuses in the cleft and binds with postsynaptic receptors which then open, inducing a postsynaptic current (PSC).

which, on release, may activate a corresponding pool of postsynaptic receptors (Walmsley *et al.*, 1998). The RRVP is replenished from a large reserve pool. The reality is likely to be more complex than this, with vesicles in the RRVP possibly consisting of a number of subpools, each in different states of readiness (Thomson, 2000b). Recycling of vesicles may also involve a number of distinguishable reserve pools (Thomson, 2000b; Rizzoli and Betz, 2005).

A model of such a synapse could itself be very complex. The first step in creating a synapse model is identifying the scientific question we wish to address. This will affect the level of detail that needs to be included. Very different models will be used if our aim is to investigate the dynamics of a neural network involving thousands of synapses compared to exploring the influence of transmitter diffusion on the time course of a miniature **excitatory postsynaptic current (EPSC)**. In this chapter, we outline the wide range of mathematical descriptions that can be used to model both chemical and electrical synapses. We start with the simplest models that capture the essence of the postsynaptic electrical response, before including gradually increasing levels of detail.

The abbreviation **IPSC**, standing for **inhibitory postsynaptic current**, is also used.

7.2 The postsynaptic response

The aim of a synapse model is to describe accurately the postsynaptic response generated by the arrival of an action potential at a presynaptic terminal. We assume that the response of interest is electrical, but it could equally be chemical, such as an influx of calcium or the triggering of a second-messenger cascade. For an electrical response, the fundamental quantity to be modelled is the time course of the postsynaptic receptor conductance. This can be captured by simple phenomenological waveforms, or by more complex kinetic schemes that are analogous to the models of membrane-bound ion channels discussed in Chapter 5.

7.2.1 Simple conductance waveforms

The electrical current that results from the release of a unit amount of neurotransmitter at time t_s is, for $t \geq t_s$:

$$I_{syn}(t) = g_{syn}(t)(V(t) - E_{syn}), \tag{7.1}$$

where the effect of transmitter binding to and opening postsynaptic receptors is a conductance change, $g_{syn}(t)$, in the postsynaptic membrane. $V(t)$ is

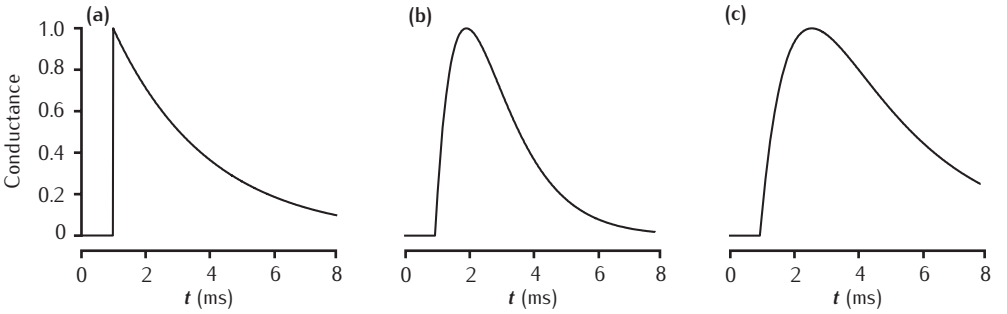

Fig. 7.2 Three waveforms for synaptic conductance: **(a)** single exponential decay with $\tau = 3$ ms, **(b)** alpha function with $\tau = 1$ ms, and **(c)** dual exponential with $\tau_1 = 3$ ms and $\tau_2 = 1$ ms. Response to a single presynaptic action potential arriving at time = 1 ms. All conductances are scaled to a maximum of 1 (arbitrary units).

the voltage across the postsynaptic membrane and E_{syn} is the reversal potential of the ion channels that mediate the synaptic current. Simple waveforms are used to describe the time course of the synaptic conductance, $g_{syn}(t)$, for the time after the arrival of a presynaptic spike, $t \geq t_s$. Three commonly used waveform equations are illustrated in Figure 7.2, in the following order, (a) single exponential decay, (b) alpha function (Rall, 1967) and (c) dual exponential function:

$$g_{syn}(t) = \overline{g}_{syn} \exp\left(-\frac{t - t_s}{\tau}\right) \tag{7.2}$$

$$g_{syn}(t) = \overline{g}_{syn} \frac{t - t_s}{\tau} \exp\left(-\frac{t - t_s}{\tau}\right) \tag{7.3}$$

$$g_{syn}(t) = \overline{g}_{syn} \frac{\tau_1 \tau_2}{\tau_1 - \tau_2} \left(\exp\left(-\frac{t - t_s}{\tau_1}\right) - \exp\left(-\frac{t - t_s}{\tau_2}\right)\right). \tag{7.4}$$

The alpha and dual exponential waveforms are more realistic representations of the conductance change at a typical synapse, and good fits of Equation 7.1 using these functions for $g_{syn}(t)$ can often be obtained to recorded synaptic currents. The dual exponential is needed when the rise and fall times must be set independently.

Response to a train of action potentials

If it is required to model the synaptic response to a series of transmitter releases due to the arrival of a stream of action potentials at the presynaptic terminal, then the synaptic conductance is given by the sum of the effects of the individual waveforms resulting from each release. For example, if the alpha function is used, for the time following the arrival of the nth spike ($t > t_n$):

$$g_{syn}(t) = \sum_{i=1}^{n} \overline{g}_{syn} \frac{t - t_i}{\tau} \exp\left(-\frac{t - t_i}{\tau}\right), \tag{7.5}$$

where the time of arrival of each spike i is t_i. An example of the response to a train of releases is shown in Figure 7.3.

A single neuron may receive thousands of inputs. Efficient numerical calculation of synaptic conductance is often crucial. In a large-scale network model, calculation of synaptic input may be the limiting factor in the speed of simulation. The three conductance waveforms considered are all solutions of the impulse response of a damped oscillator, which is given by the second

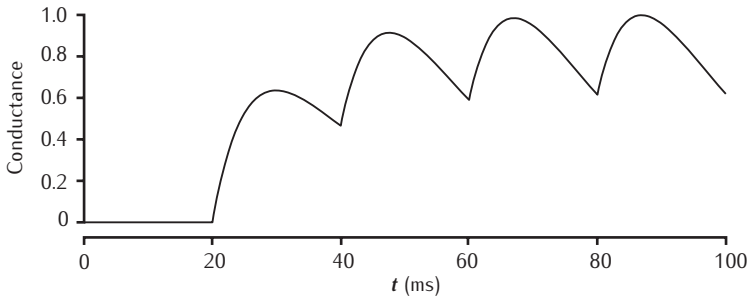

Fig. 7.3 Alpha function conductance with $\tau = 10$ ms responding to action potentials occurring at 20, 40, 60 and 80 ms. Conductance is scaled to a maximum of 1 (arbitrary units).

order ODE for the synaptic conductance:

$$\tau_1\tau_2\frac{d^2g}{dt^2}+(\tau_1+\tau_2)\frac{dg}{dt}+g=\overline{g}_{syn}x(t). \tag{7.6}$$

The function $x(t)$ represents the contribution from the stream of transmitter releases. It results in an increment in the conductance by $\overline{g}_{syn}$ if a release occurs at time t. The conductance $g(t)$ takes the single exponential form when $\tau_1 = 0$ and the alpha function form when $\tau_1 = \tau_2 = \tau$.

This ODE can be integrated using a suitable numerical integration routine to give the synaptic conductance over time (Protopapas *et al.*, 1998) in a way that does not require storing spike times or the impulse response waveform, both of which are required for solving Equation 7.5. A method for handling Equation 7.5 directly that does not require storing spike times and is potentially faster and more accurate than numerically integrating the impulse response is proposed in Srinivasan and Chiel (1993).

Voltage dependence of response

These simple waveforms describe a synaptic conductance that is independent of the state of the postsynaptic cell. Certain receptor types are influenced by membrane voltage and molecular concentrations. For example, NMDA receptors are both voltage-sensitive and are affected by the level of extracellular magnesium (Ascher and Nowak, 1988; Jahr and Stevens, 1990a, b). The basic waveforms can be extended to capture these sort of dependencies (Zador *et al.*, 1990; Mel, 1993):

$$g_{NMDA}(t)=\overline{g}_{syn}\frac{\exp(-(t-t_s)/\tau_1)-\exp(-(t-t_s)/\tau_2)}{(1+\mu[Mg^{2+}]\exp(-\gamma V))}, \tag{7.7}$$

where μ and γ set the magnesium and voltage dependencies, respectively. In this model the magnesium concentration $[Mg^{2+}]$ is usually set at a predetermined, constant level, e.g. 1 mM. The voltage V is the postsynaptic membrane potential, which will vary with time.

7.2.2 Kinetic schemes

A significant limitation of the simple waveform description of synaptic conductance is that it does not capture the actual behaviour seen at many synapses when trains of action potentials arrive. A new release of neurotransmitter soon after a previous release should not be expected to contribute as much to the postsynaptic conductance due to saturation of postsynaptic

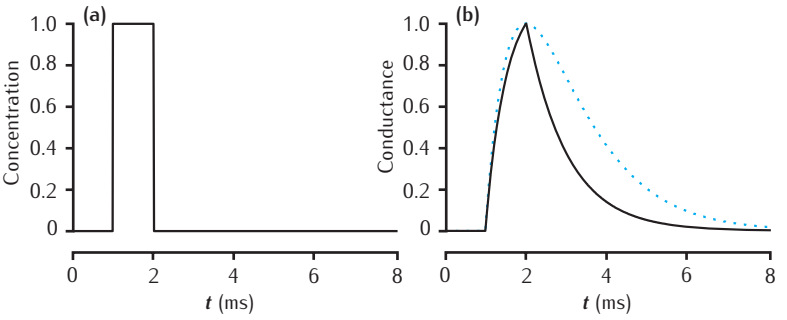

Fig. 7.4 Response of the simple two-gate kinetic receptor model to a single pulse of neurotransmitter of amplitude 1 mM and duration 1 ms. Rates are $\alpha = 1\,\text{mM}^{-1}\text{ms}^{-1}$ and $\beta = 1\,\text{ms}^{-1}$. Conductance waveform scaled to an amplitude of 1 and compared with an alpha function with $\tau = 1$ ms (dotted line).

receptors by previously released transmitter and the fact that some receptors will already be open. Certain receptor types also exhibit desensitisation that prevents them (re)opening for a period after transmitter-binding, in the same way that the sodium channels underlying the action potential inactivate. To capture these phenomena successfully, kinetic – or Markov – models (Section 5.5) can be used. Here we outline this approach. More detailed treatments can be found in the work of Destexhe *et al.* (1994b, 1998).

Basic model

The simplest kinetic model is a two-state scheme in which receptors can be either closed, C, or open, O, and the transition between states depends on transmitter concentration, [T], in the synaptic cleft:

$$\text{C} \underset{\beta}{\overset{\alpha[\text{T}]}{\rightleftharpoons}} \text{O}, \tag{7.8}$$

where α and β are voltage-independent forward and backward rate constants. For a pool of receptors, states C and O can range from 0 to 1, and describe the fraction of receptors in the closed and open states, respectively. The synaptic conductance is:

$$g_{\text{syn}}(t) = \overline{g}_{\text{syn}}\text{O}(t). \tag{7.9}$$

A complication of this model compared to the simple conductance waveforms discussed above is the need to describe the time course of transmitter concentration in the synaptic cleft. One approach is to assume that each release results in an impulse of transmitter of a given amplitude, T_{max}, and fixed duration. This enables easy calculation of synaptic conductance with the two-state model (Box 7.1). An example response to such a pulse of transmitter is shown in Figure 7.4. The response of this scheme to a train of pulses at 100 Hz is shown in Figure 7.5a. However, more complex transmitter pulses may be needed, as discussed below.

The neurotransmitter transient

The neurotransmitter concentration transient in the synaptic cleft following release of a vesicle is characterised typically by a fast rise time followed by a decay that may exhibit one or two time constants, due to transmitter uptake and diffusion of transmitter out of the cleft (Clements *et al.*, 1992; Destexhe *et al.*, 1998; Walmsley *et al.*, 1998). This can be described by the same sort of

the vesicle-state model for vesicle recycling and release (Figure 7.11) with a simple two-gate kinetic scheme for the AMPA receptor response (Figure 7.5). This shows the summed EPSCs due to 500 independent active zones which contain on average a single releasable vesicle. Note the trial-to-trial variation due to stochastic release and the interplay between facilitation of release and depletion of available vesicles.

If the trial-to-trial variation in the postsynaptic response is of interest, in addition to using a stochastic model for vesicle recycling and release, variations in **quantal amplitude**, which is the variance in postsynaptic conductance on release of a single vesicle of neurotransmitter, can be included. This is done by introducing variation into the amplitude of the neurotransmitter transient due to a single vesicle, or variation in the maximum conductance that may result (Fuhrmann *et al.*, 2002).

7.5 Long-lasting synaptic plasticity

The models detailed above incorporate aspects of short-term plasticity at synapses, such as variability in the availability of releasable vesicles and the probability of their release. Learning and memory in the brain is hypothesised to be at least partly mediated by longer-lasting changes in synaptic strength, known as **long-term potentiation** (**LTP**) and **long-term depression** (**LTD**). While short-term plasticity largely involves presynaptic mechanisms, longer-lasting changes are mediated by increases or decreases in the magnitude of the postsynaptic response to released neurotransmitter.

Models of LTP/LTD seek to map a functional relationship between pre- and postsynaptic activity and changes in the maximum conductance produced by the postsynaptic receptor pool, typically AMPARs and NMDA receptors. The biology is revealing complex processes that lead to changes in the state and number of receptor molecules (Ajay and Bhalla, 2005). As outlined in the previous chapter (Section 6.8.2), these processes involve calcium-mediated intracellular signalling pathways. Detailed models of such pathways are being developed. However, for use in network models of learning and memory, it is necessary to create computationally simple models of LTP/LTD that capture the essence of these processes, while leaving out the detail. In particular, a current challenge is to find the simplest model that accounts for experimental data on **spike-timing-dependent plasticity** (**STDP**). This data indicates that the precise timing of pre- and postsynaptic signals determines the magnitude and direction of change of the synaptic conductance (Levy and Steward, 1983; Markram *et al.*, 1997; Bi and Poo, 1998). The presynaptic signal is the arrival time of an action potential, and the postsynaptic signal is a **back-propagating action potential** (BPAP) or a synaptic calcium transient.

There are many mathematical formulations of an STDP rule. A simple one accounts for the change in synaptic strength resulting from a single pre- and postsynaptic spike pair. Suppose that a spike occurs in postsynaptic neuron j at time t^{post}, and one occurs in presynaptic neuron i at time t^{pre}. Defining the time between these spikes as $\Delta t = t^{\text{post}} - t^{\text{pre}}$, an expression

The first experimental evidence for long-lasting, activity-dependent changes in synaptic strength were obtained by Bliss and Lømo (1973). By inducing strong firing, or **tetanus**, in the granule cells of the dentate fascia of the hippocampus, Bliss and Lømo found that the amplitude of the signal due to granule cell synaptic currents remained larger after the tetanus, for hours or even days thereafter, leading to the term **long-term potentiation**. It soon became apparent that long-lasting decreases in synaptic strength could also occur in certain circumstances (Lynch *et al.*, 1977; Levy and Steward, 1979). The disparate forms of decreasing strength are known as **long-term depression**.

In addition to tetanic stimulation, it has been found that the relative timing of the presynaptic and the postsynaptic spikes affects the direction of synaptic plasticity. A synapse is more likely to be strengthened if the presynaptic neuron fires within approximately 50 milliseconds before the postsynaptic neuron; conversely, if it fires shortly after the postsynaptic neuron then the synapse is weakened. This phenomenon is referred to as **spike-timing-dependent plasticity** and is found in both developing (Zhang *et al.*, 1998) and adult synapses (Markram *et al.*, 1997; Bi and Poo, 1998).

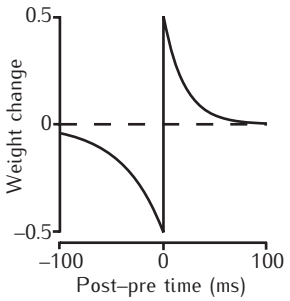

Fig. 7.13 Example STDP weight change curves. The weight is increased if the postsynaptic spike occurs at the time of, or later than, the presynaptic spike; otherwise the weight is decreased. The magnitude of the weight change decreases with the time interval between the pre- and postsynaptic spikes. No change occurs if the spikes are too far apart in time.

for the change in synaptic strength, or weight, w_{ij} is (Song *et al.*, 2000; van Rossum *et al.*, 2000):

$$\begin{aligned} \Delta w_{ij} &= A^{\mathrm{LTP}} \exp(-\Delta t/\tau^{\mathrm{LTP}}) \quad \text{if } \Delta t \geq 0 \\ \Delta w_{ij} &= -A^{\mathrm{LTD}} \exp(\Delta t/\tau^{\mathrm{LTD}}) \quad \text{if } \Delta t < 0. \end{aligned} \tag{7.35}$$

These weight change curves are illustrated in Figure 7.13. The parameters A^{LTP}, A^{LTD}, τ^{LTP} and τ^{LTD} can be determined experimentally. The data of Bi and Poo (1998) are well fit with $\tau^{\mathrm{LTP}} = 17$ ms and $\tau^{\mathrm{LTD}} = 34$ ms (van Rossum *et al.*, 2000). The magnitude of LTP, A^{LTP}, often is greater than that of LTD, but it is small for synapses that are already strong. In a synaptic model, the weight w_{ij} could be used as a scaling factor for the maximum postsynaptic receptor conductance, $\overline{g}_{\mathrm{syn}}$ (Section 7.2).

More complex models attempt to account for data from stimulation protocols that include triplets or more physiological patterns of spikes (Abarbanel *et al.*, 2003; Castellani *et al.*, 2005; Rubin *et al.*, 2005; Badoual *et al.*, 2006). The simplest such model is a generalisation of the simple spike pair model (Equation 7.35) that treats the weight change as the linear sum of changes due to individual spike pairs within a sequence of pre- and postsynaptic spikes (Badoual *et al.*, 2006). It relates the sequence of spike times to the rate of change in synaptic strength w_{ij} between presynaptic neuron i and postsynaptic neuron j, via the equation:

$$\begin{aligned} \frac{\mathrm{d}w_{ij}}{\mathrm{d}t} = &\sum_k A^{\mathrm{LTP}} \exp(-(t - \tilde{t}^{\mathrm{pre}})/\tau^{\mathrm{LTP}}) \delta(t - t_k^{\mathrm{post}}) \\ &- \sum_l A^{\mathrm{LTD}} \exp(-(t - \tilde{t}^{\mathrm{post}})/\tau^{\mathrm{LTD}}) \delta(t - t_l^{\mathrm{pre}}). \end{aligned} \tag{7.36}$$

The sum k is over all postsynaptic spikes, occurring at times t_k^{post}, and the sum l is over all presynaptic spikes. On occurrence of a postsynaptic spike, the weight is increased as an exponentially decaying function of the immediately preceding presynaptic spike time $\tilde{t}^{\mathrm{pre}}$. Similarly, the weight is decreased when a presynaptic spike occurs, as an exponentially decaying function of the immediately preceding postsynaptic spike time $\tilde{t}^{\mathrm{post}}$.

In reality, weight changes to general pre- and postsynaptic spike trains do not seem to be simple linear sums of the changes expected from individual spike pairs (Froemke and Dan, 2002). Further phenomenological components can be added to this simple model to incorporate effects such as weight saturation and spike triplet interactions, for example (Badoual *et al.*, 2006):

$$\begin{aligned} \frac{\mathrm{d}w_{ij}}{\mathrm{d}t} = \epsilon_i \epsilon_j \Bigg[&(w^{\mathrm{LTP}} - w_{ij}) \sum_k A^{\mathrm{LTP}} \exp(-(t - \tilde{t}^{\mathrm{pre}})/\tau^{\mathrm{LTP}}) \delta(t - t_k^{\mathrm{post}}) \\ &- (w_{ij} - w^{\mathrm{LTD}}) \sum_l A^{\mathrm{LTD}} \exp(-(t - \tilde{t}^{\mathrm{post}})/\tau^{\mathrm{LTD}}) \delta(t - t_l^{\mathrm{pre}}) \Bigg]. \end{aligned} \tag{7.37}$$

Previous spiking history seems to suppress the magnitude of change for the current spike pair (Froemke and Dan, 2002), and this is captured by two 'suppression' factors, $\epsilon_i = 1 - \exp(-(t_i - t_{i-1})/\tau_i^s)$ and $\epsilon_j = 1 - \exp(-(t_j - t_{j-1})/\tau_j^s)$, which are decaying functions of the time interval between the

previous and current spikes in pre- and postsynaptic neurons i and j, respectively. Weights are now limited to be within the range $w^{\text{LTD}} \leq w_{ij} \leq w^{\text{LTP}}$.

Rather than pre- and postsynaptic spike times, the major determinant of long-term synaptic changes is the postsynaptic calcium levels resulting from pre- and postsynaptic activity via calcium entry through NMDA- and voltage-gated calcium channels (Ajay and Bhalla, 2005). Both the magnitude and time course of calcium transients determine the sign and magnitude of synaptic weight changes. Badoual *et al.* (2006) present a simple, phenomenological intracellular signalling scheme to model the mapping from calcium to weight changes. An enzyme, K, mediates LTP in its activated form, K^*, which results from binding with calcium:

$$K + 4Ca^{2+} \underset{k^-}{\overset{k^+}{\rightleftharpoons}} K^*. \tag{7.38}$$

The LTD enzyme, P, is activated by two other enzymes, M and H, that are activated by calcium, and neurotransmitter, T, respectively:

$$\begin{aligned} M + Ca^{2+} &\underset{m^-}{\overset{m^+}{\rightleftharpoons}} M^* \\ H + T &\underset{h^-}{\overset{h^+}{\rightleftharpoons}} H^* \\ M^* + H^* + P &\xrightarrow{p^+} P^*. \end{aligned} \tag{7.39}$$

The percentage increase in synaptic weight (maximum conductance) is proportional to K^* and the percentage decrease is proportional to P^*, with the total weight change being the difference between these changes. This model specifies that the sign and magnitude of a weight change is determined by the peak amplitude of a calcium transient. It captures the basic phenomena that lower levels of calcium result in LTD, whereas higher levels result in LTP. More biophysically realistic, but computationally more complex models, that attempt to capture the relationship between postsynaptic calcium transients and changes in synaptic strength, are considered in Section 6.8.2.

7.6 Detailed modelling of synaptic components

We have concentrated on models that describe synaptic input for use in either detailed compartmental models of single neurons or in neural networks. Modelling can also be used to gain greater understanding of the components of synaptic transmission, such as the relationship between presynaptic calcium concentrations and vesicle recycling and release (Zucker and Fogelson, 1986; Yamada and Zucker, 1992; Bennett *et al.*, 2000a, b), or the spatial and temporal profile of neurotransmitter in the synaptic cleft (Destexhe and Sejnowski, 1995; Barbour and Häusser, 1997; Rao-Mirotznik *et al.*, 1998; Smart and McCammon, 1998; Franks *et al.*, 2002; Coggan *et al.*, 2005; Sosinsky *et al.*, 2005). This is illustrated in Figure 7.14.

Such studies typically require modelling molecular diffusion in either two or three dimensions. This can be done using the deterministic and

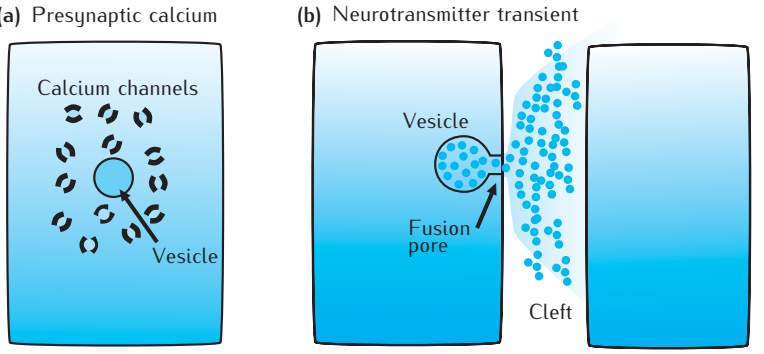

Fig. 7.14 **(a)** Spatial distribution of voltage-gated calcium channels with respect to location of a docked vesicle. **(b)** Spatial and temporal profile of neurotransmitter in the synaptic cleft on release of a vesicle.

stochastic approaches outlined in Chapter 6 in the context of modelling intracellular signalling pathways. Deterministic models calculate molecular concentrations in spatial compartments and the average diffusion between compartments (Zucker and Fogelson, 1986; Yamada and Zucker, 1992; Destexhe and Sejnowski, 1995; Barbour and Häusser, 1997; Rao-Mirotznik *et al.*, 1998; Smart and McCammon, 1998). Stochastic models track the movement and reaction state of individual molecules (Bennett *et al.*, 2000a, b; Franks *et al.*, 2002). Increasingly, spatial finite element schemes based on 3D reconstructions of synaptic morphology are being employed (Coggan *et al.*, 2005; Sosinsky *et al.*, 2005). The simulation package MCELL (Stiles and Bartol, 2001) is specifically designed for implementing stochastic models based on realistic morphologies (Appendix A.1.2).

7.7 Gap junctions

Though first identified in invertebrate and vertebrate motor systems (Furshpan and Potter, 1959; Auerbach and Bennett, 1969), it is now recognised that many neurons, including those in the mammalian central nervous system (Connors and Long, 2004), may be connected by purely electrical synapses known as **gap junctions**. These electrical connections are typically dendrite-to-dendrite or axon-to-axon and are formed by channel proteins that span the membranes of both connected cells (Figure 7.15a). These channels are permeable to ions and other small molecules, and allow rapid, but attenuated and slowed exchange of membrane voltage changes between cells (Bennett and Zukin, 2004). Gap junctions between cells of the same type usually are bidirectional, but junctions between cells of different types often show strong rectification, with depolarisations being transferred preferentially in one direction and hyperpolarisations in the other. This is due to the different cells contributing different protein subunits at either side of the junction (Marder, 2009; Phelan *et al.*, 2009). Gap junction conductance can also be modulated by various G protein-coupled receptors, leading to long-lasting changes in coupling strength as the result of neuronal activity (Bennett and Zukin, 2004), equivalent to the long-lasting changes seen at chemical synapses.

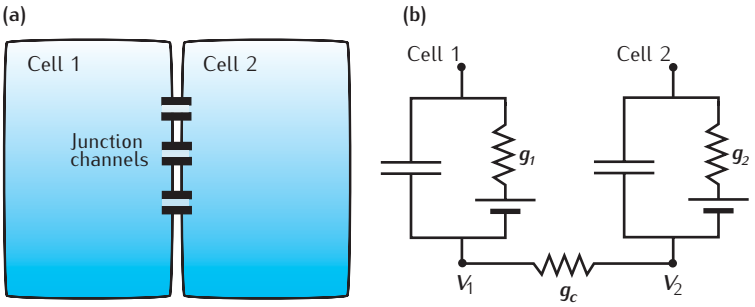

Fig. 7.15 **(a)** Schematic of a gap junction connection between two apposed neurites (dendrites or axons), with **(b)** the equivalent electrical circuit.

A simple gap junction model assumes a particular fixed, symmetric permeability of the gap junction channels. Thus the electrical current through a gap junction is modelled as being strictly ohmic, with a coupling conductance g_c. The current flowing into each neuron is proportional to the voltage difference between the two neurons at the point of connection (Figure 7.15b):

$$\begin{aligned} I_1 &= g_c(V_2 - V_1) \\ I_2 &= g_c(V_1 - V_2). \end{aligned} \tag{7.40}$$

An example of the effect of a gap junction between two axons is shown in Figure 7.16. The gap junction is half-way along the two axons, and an action potential is initiated at the start of one axon. If the gap junction is sufficiently strong then the action potential in the first axon can initiate an action potential in the second axon, which then propagates in both directions along this axon.

Even this simple connection between two neurons can lead to complex effects. The response of one neuron to the voltage change in the other can be quite asymmetric between neurons, despite a symmetric coupling conductance, if the two neurons have different cellular resistances (or, equivalently, conductances). For the circuit shown in Figure 7.15b, consider current being injected into cell 1 so that it is held at voltage V_1, relative to its resting membrane potential. Kirchhoff's law for current flow stipulates that the current flowing into point V_2 must equal the current flowing out, so that:

$$(V_1 - V_2)g_c = V_2 g_2. \tag{7.41}$$

Rearranging this equation gives a coupling coefficient that describes the relative voltage seen in cell 2 for a given voltage in cell 1:

$$\frac{V_2}{V_1} = \frac{g_c}{g_2 + g_c}. \tag{7.42}$$

Clearly, V_2 is always less than V_1, and the attenuation will be only small if the conductance of cell 2 is low (the cell has a high input resistance), relative to the coupling conductance. Similarly, if cell 2 is held at V_2, then the

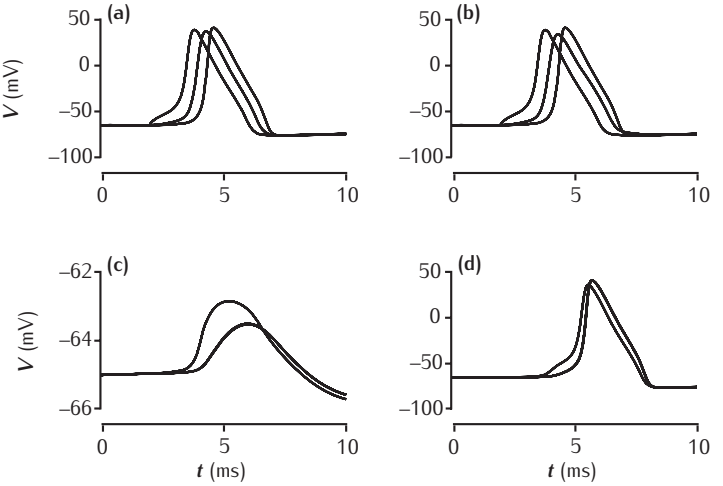

Fig. 7.16 Simulated action potential travelling along two axons that are joined by a gap junction half-way along their length. Membrane potentials are recorded at the start, middle and end of the axons. **(a, b)** Axon in which an action potential is initiated by a current injection into one end. **(c)** Other axon, with a 1 nS gap junction. **(d)** Other axon, with a 10 nS gap junction. Axons are 100 μm long, 2 μm in diameter with standard Hodgkin–Huxley sodium, potassium and leak channels.

attenuation in V_1 is given by:

$$\frac{V_1}{V_2} = \frac{g_c}{g_1 + g_c}. \tag{7.43}$$

If $g_1 \neq g_2$, then the attenuation across the gap junction is not symmetric for voltage changes in cell 1 or cell 2.

The above derivation of coupling attenuation assumes that the cellular conductances are fixed. However, changes in membrane potential are often accompanied by, or result from, changes in membrane conductance due to the opening or closing of ion channels. This can result in a fixed, symmetric coupling also being somewhat rectifying, with hyperpolarisations being less attenuated than depolarisations, due to the decrease in cellular membrane resistance associated with depolarisations. This is a different form of rectification than that resulting from an asymmetric subunit structure of the gap junction proteins.

7.8 Summary

The chemical synapse is a very complex device. Consequently, a wide range of mathematical models of this type of synapse can be developed. When embarking on developing such a model it is essential that the questions for which answers will be sought by the use of the model are clearly delineated.

In this chapter we have presented various models for chemical synapses, ranging from the purely phenomenological to models more closely tied to the biophysics of vesicle recycling and release and neurotransmitter gating of postsynaptic receptors. Along the way we have highlighted when different types of model may be appropriate and useful.

Many of the modelling techniques are the same as those seen in the previous two chapters. In particular, the use of kinetic reaction schemes and their equivalent ODEs. Stochastic algorithms have been used when the ODE approach is not reasonable, such as for the recycling and release of small numbers of vesicles at an active zone.